Journal of Thermal Analysis and Calorimetry, Vol. 90 (2007) 3, 627–638

THE LOW TEMPERATURE SYNTHESIS OF METAL OXIDES BY NOVEL HYDRAZINE METHOD

K. S. Rane[*]*, H. Uskaikar, R. Pednekar and R. Mhalsikar*

Department of Chemistry, Goa University, Goa 403206, India

The hydroxide, oxalate and citrate precursors of the metal oxides such as γ-Fe_2O_3, $(MnZn)Fe_2O_4$, $Cu(K)Fe_2O_4$, $BaTiO_3$, $La(Sr)MnO_3$, $La(Sr)AlO_3$, $La/Gd(Ca/Ba/Sr)CoO_3$, and anatase TiO_2 on modifications with the hydrazine decompose at low temperatures give single phase oxides of superior properties, while the complexes without such modification require higher temperatures for achieving the phases. The hydrazine released at lower temperatures reacts with the oxygen in the atmosphere, $N_2H_4+O_2 \rightarrow N_2+2H_2O$; $\Delta H = -625$ kJ mol^{-1}, and liberates enormous energy that is sufficient for the oxidative decomposition of the complexes now devoid of hydrazine. Such extra energy is not available in the case of the precursors without such modifications. The reaction products of hydrazine oxidation provide desired partial pressure of moisture needed for the stabilization of γ-Fe_2O_3. Also, the nitrogen that is formed in the reaction of hydrazine with oxygen gets trapped in the lattice of TiO_2 giving yellow color nitrogen doped $TiO_{2-x}N_x$ photocatalyst. Thus, hydrazine method of preparation has many advantages in the preparation of metal oxides of superior properties.

Keywords: *hydrazinate precursors, hydrazine, N-doped oxide, thermal decomposition*

Introduction

The recent arousal of interest in nanosize oxide materials is a challenge to the synthetic chemists as it is a material preparation that matters a lot, that too, in the reproducible manner. The development of nanostructure materials with unique parameters is impossible without mastering techniques for producing such weakly agglomerated powders with mean size of 10–15 nm. However, the chemists have always been active in synthesis of submicron size materials of high surface area active oxides that require say, for catalytic applications or for further sintering them into well dense electric, magnetic and optical materials. But, because of their coarse nature these submicron size particles suffer in giving properties that are grain size controlled, such as electrical conductance. The continued synthetic strategies adopted by the chemists have enabled them to achieve materials of average particle size of 100 nm through techniques such as sol-gel, spray-pyrolysis, pulsed laser ablation, chemical vapor deposition, thermal decomposition etc., whereas gas phase methods have resulted into nanosize particles. Then, these advanced methods of preparation of nanosize materials need metal oxide precursors, such as metalloorganic compounds, which are expensive and processes require stringent conditions. Hence, it is always better to explore further the conventional processes, such as thermal decomposition of easily decomposable precursors of oxides. Lowering of temperature of decomposition has better chance to obtain the desired oxides in very fine particle size which has been realized by the chemists over the years, but it needs furthering of research in this area to get precursors of very low decomposition temperature. And, we have been considering this aspect of synthesizing oxides of spinel, perovskite, anatase structure in our laboratories [1–9] using novel hydrazine modified precursors. Our objective in this type of research was to prepare electric, magnetic, sensing and photoconducting materials of submicron size of average 100–150 nm from low temperature thermal decomposition of metal and mixed metal carboxylates, hydroxides. However, the modification of these precursors by hydrazination enabled us to further decrease the decomposition temperature resulting into sub-submicron size particles of average 50–75 nm with low agglomeration as compared to those obtained without such modifications. Since these are easily decomposable metal complexes, it is but natural to use the thermal analysis techniques to assess their thermal decomposition paths. Here in the present paper we are compiling our results of thermal analysis of metal oxalates, citrates, hydroxides and their hydrazinate precursors of the oxide systems such as, γ-Fe_2O_3, $(MnZn)Fe_2O_4$, $CuFe_2O_4$, $Cu(K)Fe_2O_4$ $BaTiO_3$, $La(Sr)MnO_3$, $La(Sr)AlO_3$, $La/Gd(Ca/Ba/Sr)CoO_3$, and anatase TiO_2.

Hydrazine method of preparation is a novel way of synthesizing materials of desired structure and properties at lower temperatures. For instance, ferrous

* Author for correspondence: ksrane@unigoa.ac.in; ksrane@rediffmail.com

1388–6150/$20.00

Akadémiai Kiadó, Budapest, Hungary
Springer, Dordrecht, The Netherlands

oxalate dihydrate, $FeC_2O_4{\cdot}2H_2O$, decomposes in air to hexagonal corundum nonmagnetic α-Fe_2O_3, while the hydrazinated oxalate, $FeC_2O_4{\cdot}2N_2H_4$, auto-catalytically decomposes to cubic magnetic γ-Fe_2O_3 [1–2] and similar observations were also made for other iron(II) carboxylates such as ferrous-fumarate/succinate/maleate/malate/malonate [3]. Iron hydroxides modified by hydrazine too showed the easy formation of γ-Fe_2O_3 [4]. Ni–Zn–Ferrite [5] and $MgFe_2O_4$ [6] synthesized from oxalate precursors that modified by hydrazine showed better magnetic properties. Dielectric properties of $MgFe_2O_4$ [7] from oxalate hydrazinate and semiconducting properties of γ-Fe_2O_3 from iron hydroxides modified by hydrazination [8] are found to be superior as compared to the oxide prepared from the unhydrazinated compound. The titanium hydroxide and titanium oxalate decompose to white pigment grade anatase TiO_2, while their hydrazinates yield yellow color visible light sensitive nitrogen doped $TiO_{2-x}N_x$ photo-catalyst [9] showing improved electrical properties [10]. In hydrothermal route for synthesizing SnO_2 quantum dots [11] the use of hydrazine hydrate is most critical in achieving the particles in a small range of 2.3–3.1 nm. In room temperature preparation of novel $Cu_{2-x}Se$ nanotubes in organic solvents the presence of hydrazine hydrate aids the formation [12]. A novel low-temperature sol-gel based process in the synthesis of crystalline in the Al–N–O system involves a reaction between aluminum tri-sec-butoxide with hydrazine hydrate [13] in the acetonitrile and chloroform medium. Conventional high temperature method of preparation of CoS has been brought down to low temperature by hydrazine assisted synthetic process [14].

Experimental

Synthesis

Oxalate/citrate precursors

The oxalate precursors of spinels, MFe_2O_4 (M=Cu/Mn–Zn/K); perovskites, La/Gd $(M^{II})MO_3$ (M=Mn/Co/Al; M^{II}=Ca/Sr/Ba) and $BaTiO_3$, and TiO_2 were synthesized by standard methods. Commercial metal chlorides and oxalic acid/citric acid were used for the synthesis. However, in the preparation of the oxalate precursor of TiO_2 a freshly prepared titanium chloride from commercial TiO_2 was used. Here the commercial titania was fused with KOH in Ni crucible and then by adding conc. HCl, potassium was removed as KCl and the fresh titanium chloride that now obtained was treated with ammonia to get titanium hydroxide. The titanium hydroxide on acidifying yielded a very pure titanium chloride.

Hydroxide precursors

Titanium hydroxide was prepared by taking titanium iso-propoxide in iso-propanol and adding slowly to a large quantity of water. Titanium hydroxide was also prepared by adding ammonium hydroxide to titanium chloride.

Modification of oxalate/citrate/hydroxide precursors by hydrazine

a) Under hydrazine (UH) method: equilibration: The oxalate and hydroxide precipitates were spread over a Petri dish and placed in closed vessel containing 99.9% hydrazine hydrate. The hydrazine intake was monitored by titrimetrically using KIO_3 titrant [15].

b) Synthetic hydrazine (SH) method: In another method of preparation of hydrazine modified precursors, the oxalic acid and hydrazine hydrate were first stirred well under inert nitrogen atmosphere in 3 necked retort and to the mixture a freshly prepared metal chloride solution was rundown to precipitate out the hydrazinated complexes.

Methods

Chemical, isothermal mass loss analysis: formula fixation

For proposing chemical formula for the oxalate, hydroxide, citrates and their hydrazinate complexes chemical estimation of metals, oxalate and hydrazine were done as per the standard methods described in Vogel [15]. Total mass loss measurements were done in a muffle furnace. Infrared analyses were done on Shimadzu IR Prestige-21.

Thermal analysis

Thermogravimetric analysis (TG) and differential scanning calorimetric (DSC) analysis were preformed on NETZSCH DSC-DTA-TG STA 409PC. The heating rate was fixed at 10°C min^{-1}. The analyses were done in the flowing air atmosphere in most of the cases, and in few cases nitrogen gas was used.

X-ray diffraction (XRD), SEM/TEM and XPS studies

The decomposed products were identified from X-ray diffraction (XRD) studies on ITAL APD 2000 using CuK_α radiation (λ=1.5418 Å) and Ni filter. The d_{hkl} values obtained by XRD were matched with the JCPDS/ICDD Card of individual oxide systems. Scanning electron microscopic (SEM) studies were conducted on HITACHI S-4500. Transmission electron micrographs (TEM) were recorded with JEOL-JEM 100SX microscope, working at 100 kV

accelerating voltage. X-ray photoelectron spectroscopy (XPS) measurements were carried out over a Kratas Axis Spectrometer at a vacuum of $3 \cdot 10^{-9}$ Torr with non-monochromatic MgK_α radiation.

Nitrogen estimation, dielectric property, saturation magnetization, electronic conductivity

The amount of nitrogen in TiO_2 was determined using the oxygen-nitrogen analyzer [16] (HIROBA, EMGA, 2800). Dielectric constant of $BaTiO_3$ was measured as a function of temperature in a two-probe set up in a constant frequency of 1 KHz and that of $LaAlO_3$ at different temperatures and frequencies. Saturation magnetization of magnetic $CuFe_2O_4$ in emu/g was carried out on the instrument supplied by M/s. Arun Electronics, Mumbai, [17] using Ni as standard. Electronic conductivity of $LaCoO_3$ system was measured by Van der Pauw method [18]

Results and discussion

Chemical formulas

The observed percentage of oxalate, citrate, hydrazine and total mass loss of the complexes are compiled in the Table 1. From these values formula for each complex is proposed and the calculated values given in the bracket are found to match well with observed ones. The infrared (IR) spectra of all these complexes were recorded in the range of 4000–400 cm^{-1} and important peaks have been listed in the Table 1. The carboxylate complexes show absorption frequencies in the range 3000–3600 cm^{-1} which may be attributed to O–H frequency (ν_{OH}) of water, but more broadening of the peaks observed for the hydrazinated complexes which is due to the N–H stretching (ν_{NH}) frequencies. The carboxylate groups have their asymmetric and symmetric stretching frequencies, ν_{ooc} asym/sym, in the region 1640–1610 and 1450–1375 cm^{-1}, respectively. The observed N–N stretching (ν_{NN}) frequencies in the region ~980 cm^{-1} indicate the presence of hydrazine, N_2H_4, either as $N_2H_5^+$ or as a bidentate bridging $H_2N–NH_2$ [19–21]. The NH_2 bending vibrations at ~1600 cm^{-1} (which could include contributions from δ_{NH}) and 1540 cm^{-1} [22–24] although merged in the hydrazinate complexes of the carboxylates, band positions in this range clearly indicate its presence in the titanium hydroxides. The fundamental stretching of hydroxyl (free or bonded) frequencies in the range 3600–3100 cm^{-1} in the titanium hydroxide are observed in combination with another peak ~1630 cm^{-1} due to the bending vibrations of coordinated H_2O as well as Ti–OH [26]. However, a peak ~1400 cm^{-1} that observed has been assigned to [26] the oxyhydroxide. A broad stretching vibration mode of OH group at 3425 cm^{-1} and corresponding bending vibration band at 1637 cm^{-1} observed within a TiO_2 sol-gel [27] occurred during the gelling of the titanium alkoxide. An additional band at 1389 cm^{-1} that had been assigned to an asymmetric bending vibration of C–H [27] due to the presence of organic moiety is not found in our titanium hydroxide prepared by the hydrolysis of titanium isopropoxide, Fig. 1a, but a broad band centered ~3340 cm^{-1} due to stretching vibration and corresponding bending vibration band at 1641 cm^{-1} have appeared. On the other hand, the hydroxide prepared from freshly prepared titanium chloride by precipitating with ammonia, shows, Fig. 1b, an additional band at 1427 cm^{-1} along with very broad band centered ~3240 and 1631 cm^{-1}. However, infrared spectra recorded on the hydroxides prepared from the titanium chloride and heat treated at different temperatures up to 800°C, Figs 1a and b, indicate that the band at 1427 cm^{-1} vanishes and the broad band centered ~3240 cm^{-1} narrows at 300°C and finally at 800°C the ~3240 cm^{-1} band shows its weak presence.

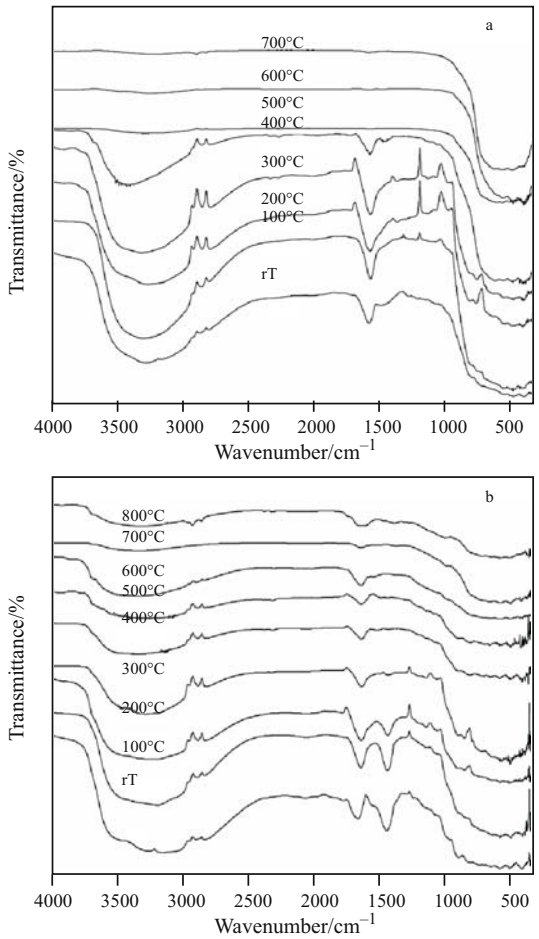

Fig. 1 Temperature variation of FTIR of titanium hydroxide obtained from a – titanium isopropoxide, b – titanium chloride

Table 1 Analytical and infrared data (experimental)

Proposed chemical formula	Total mass loss/%	C_2O_4/ %	N_2H_4/ %	ν_{OH}/ ν_{NH}	IR peak/cm^{-1} ν_{ooc}/ asym/sym δ_{NH}	ν_{NN}/ δ_{NN}
$LaAl(C_2O_4)_3 \cdot 10H_2O$	64.5	43.0	–	3200–3400	1650/1325	–
	(64.9)	(43.3)				
$LaAl(C_2O_4)_3 \cdot N_2H_4 \cdot 3H_2O$	64.9	51.3	6.7	3200–3500	1625/1325	960
	(64.7)	(51.2)	(6.2)			
$La_{0.65}Sr_{0.35}Al(C_2O_4)_3 \cdot 2N_2H_4$	68.2	44.0	11.0	3200–3600	1625/1350	960
	(68.2)	(43.9)	(10.6)			
$La_{0.7}Sr_{0.3}Mn(C_2O_4)_3 \cdot 2N_2H_4 \cdot 15H_2O$	70.9	34.8	8.2	3200–3550	1625/1350	960
	(70.8)	(34.0)	(8.2)			
$GdCo(C_6H_5O_7)_2 \cdot 2H_2O$	75.8	–	–	3400	1600/1400	–
	(75.7)					
$GdCo(C_6H_5O_7)_2 \cdot 4N_2H_4$	74.0	–	17.6	3300–3500	1700/1400	960
	(73.2)		(17.7)			
$Gd_{0.8}Ca_{0.2}Co(C_6H_5O_7)_2 \cdot 10H_2O$	74.0	–	–	3300–3500	1700/1400	
	(74.3)					
$Gd_{0.8}Ca_{0.2}Co(C_6H_5O_7)_2 \cdot 4N_2H_4$	72.5	–	17.9	3300–3500	1750/1400	980
	(72.8)		(18.1)			
$Gd_{0.8}Ba_{0.2}Co(C_6H_5O_7)_2 \cdot 10H_2O$	78.4	–	–	3300–3500	1750/1400	–
	(79.1)					
$Gd_{0.8}Ba_{0.2}Co(C_6H_5O_7)_2 \cdot 4N_2H_4$	76.0		13.6	3300–3500	1750/1400	980
	(75.2)		(13.9)			
$Ba[TiO(C_2O_4)_2] \cdot 6H_2O$	52.0	59.0	–	3600–3400	1680/1420	
	(51.9)	(59.8)	–			
$Ba[TiO(C_2O_4)_2] \cdot 7N_2H_4$	62.7	29.1	37.0	3500–3300	1680/1425	1084
	(61.2)	(29.2)	(37.2)			
$(NH_4)_2TiO(C_2O_4)_2 \cdot H_2O$	72.2	59.2	–	2800–3500	1600/1300	–
	(72.8)	(59.8)				
$(N_2H_5)_2[TiO(C_2O_4)_2] \cdot N_2H_4$ (UH)	76.8	52.1	9.8	2200–3200	1600/1300	980
	(76.3)	(52.1)	(9.4)	Very broad		
$(N_2H_5)_2[TiO(C_2O_4)_2] \cdot 3N_2H_4$ (SH)	79.4	43.2	23.5	2600–3200	1700/1300	980
	(79.9)	(43.8)	(23.8)	Very broad	1500	
$TiO(OH)_2 \cdot 2.5H_2O$	44.1	–	–	3200–3600	1400	–
	(45.0)	–	–		1630	
$TiO(OH)_2 \cdot N2H_4$ (UH)	40.0	–	24.1	3200–4000	1400	–
	(39.0)	–	(24.6)	–	1630	
$TiO(OH)_2 \cdot 4N_2H_4$ (SH)	66.0	–	56.5	3200–4000	1400	–
	(65.0)	–	(56.6)	–	1630	
$CuFe_2(C_2O_4)_3 \cdot 8H_2O$	59.4	45.9	–	3500–3200	1650/1450	–
	(59.0)	(45.2)				
$CuFe_2(C_2O_4)_3 \cdot 3N_2H_4 \cdot 4H_2O$	59.9	46.0	16.4	3500–3200	1650/1450	980
	(59.8)	(44.3)	(16.1)			
$Cu_{0.9}K_{0.1}Fe_2(C_2O_4)_3 \cdot 9H_2O$	61.6	43.7	–	3500–3200	1650/1450	–
	(60.2)	(43.3)				
$Cu_{0.9}K_{0.1}Fe_2(C_2O_4)_3 \cdot 5N_2H_4 \cdot 9H_2O$	64.5	43.7	24.8	3500–3200	1650/1350	980
	(64.4)	(39.3)	(23.9)			

Table 1 Continued

Proposed chemical formula	Total mass loss/%	C_2O_4/ %	N_2H_4/ %	ν_{OH}/ ν_{NH}	IR peak/cm^{-1} ν_{ooc}/ asym/sym δ_{NH}	ν_{NN}/ δ_{NN}
$Mn_{0.65}Zn_{0.35}Fe_2(C_2O_4)_3 \cdot 8H_2O$	59.4	46.0	–	3500–3200	1650/1450	–
	(60.2)	(45.8)				
$Mn_{0.65}Zn_{0.35}Fe_2(C_2O_4)_3 \cdot 3N_2H_4 \cdot 5H_2O$	61.5	28.0	15.3	3500–3200	1650/1350	980
	(62.2)	(28.3)	(15.5)			
$FeC_2O_4 \cdot 2H_2O$	55.8	49.1	–	3500	1650/1350	–
	(55.6)	(48.9)				
$FeC_2O_4 \cdot 2N_2H_4$	61.8	43.1	31.0	3350	1650–1350	980
	(61.5)	(42.3)	(30.8)			

The numbers in parantheses mean calculated data

But the band at 1631 cm^{-1} also persists at 800°C, while in the case of the hydroxide from alkoxide the bands ~3340 and 1641 cm^{-1} vanish at 500°C. These observations suggest that the additional peak at 1427 cm^{-1} and a broad band centered ~3240 cm^{-1} in the titanium hydroxide prepared by precipitating titanium chloride with ammonia may be due to the presence of ammonia in the precipitate.

On the basis of the results of IR and chemical analysis (presented in Table 1) it appears that hydrazine complexes are formed. The chemical formulas for the GdCo complexes were difficult to ascertain, and an adduct type [25] hydrazine complex of the citrates may be considered in the following manner: $GdCo(C_6H_5O_7)_2 \cdot 4N_2H_4$, $Gd_{0.8}Ca_{0.2}Co(C_6H_5O_7)_3 \cdot 4N_2H_4$, $Gd_{0.8}Ba_{0.2}Co(C_6H_5O_7)_3 \cdot 3N_2H_4$.

Thermal analysis

TG-DSC traces of individual samples have been analyzed separately to record the different peak temperatures and corresponding temperature ranges of mass losses. However, for the purpose of the comparison of the thermal paths of hydrazinate and unhydrazinate precursors of each system, the DSC/TG traces have been shown in one figure. Here, note that the numerical for both the temperature and DSC (mW/mg)/% mass loss axes are arbitrary, not to the scale. The peak temperatures shown are from the individual traces

Spinel systems

$CuFe_2O_4$ system

The TG-DSC traces of $CuFe_2(C_2O_4)_3 \cdot 8H_2O$ (CuFe_oxalate) and $CuFe_2(C_2O_4)_3 \cdot 3N_2H_4 \cdot 4H_2O$ (CuFe_oxalate_hyd) are shown in Fig. 2a. The oxalate complex indicates a sharp endothermic peak at ~204°C which is immediately followed by a broad intense exothermic reaction in the range 204–332°C with a peak at ~307°C, while its hydrazinate complex shows an exothermic peak at ~146°C and another exotherm between 185 and 330°C with a peak at ~270°C. The TG mass loss curves for both the complexes between room temperature (rT) and 330°C show two steps decomposition, but, the hydrazine complex clearly shows measurable two-step mass loss. The first step in the oxalate complex is dehydration which is then followed by decarboxylation. The first step on mass loss in hydrazine complex is found to be due to dehydrazination as confirmed by the absence of hydrazine in the complex that had been isothermally

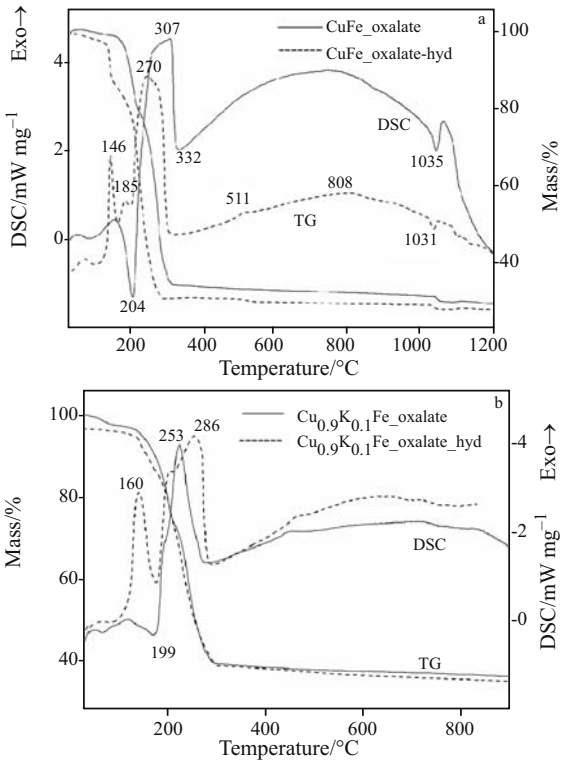

Fig. 2 TG/DSC plots of a – copper iron oxalate/oxalate hydrazinate, b – potassium doped copper iron oxalate/oxalate hydrazinate

decomposed separately at ~130°C. The second step in the hydrazine complex is due to dehydration and decarboxylation. Thus, in the temperature range rT-330°C, the dehydration is followed by decarboxylation in $CuFe_2(C_2O_4)_3{\cdot}8H_2O$, while in the hydrazinate complex, $CuFe_2(C_2O_4)_3{\cdot}3N_2H_4{\cdot}4H_2O$ the sequence is dehydrazination-dehydration-decarboxylation. At ~330°C both the complexes show almost complete decomposition as observed in the TG trace, beyond this temperature there is no measurable mass change, however, DSC shows a broad exothermic up to 1020°C and then there appears an endothermic peak ~1030°C in both samples. The TG trace which was showing a negligible mass loss till 1020°C suddenly indicates a depression in the mass loss and corresponding to that there appears an endotherm ~1030°C. From the XRD studies, Fig. 3, the thermal product of $CuFe_2(C_2O_4)_3{\cdot}3N_2H_4{\cdot}4H_2O$ that had been isothermally heated separately ~290°C indicated a single phase $CuFe_2O_4$ formation, while ~330°C is required for $CuFe_2(C_2O_4)_3{\cdot}8H_20$ to form the spinel. Hydrazine modification of the oxalate precursor enables to prepare the spinel at low temperature.

K-doped $CuFe_2O_4$

The DCS-TG traces of potassium doped oxalate and hydrazinate complexes, $Cu_{0.9}K_{0.1}Fe_2(C_2O_4)_3{\cdot}9H_2O$, ($Cu_{0.9}K_{0.1}$_oxalate), $Cu_{0.9}K_{0.1}Fe_2(C_2O_4)_3{\cdot}5N_2H_4{\cdot}9H_2O$, ($Cu_{0.9}K_{0.1}$_oxalate_hyd) are shown in Fig. 2b. The oxalate after showing a weak endothermic peak ~199°C immediately indicates an intense exothermic process with peak centered at ~253°C, while the hydrazine complex decomposes with exothermic process with peaks situated at ~160 and 286°C. Although the thermal decomposition leading to ferrite formation in both the cases is completed at ~300°C, the $Cu_{0.9}K_{0.1}Fe_2O_4$ obtained from the hydrazine complex showed single spinel phase, Fig. 3. Magnetic characteristic such as saturation magnetization value of 28.5 emu g^{-1} is observed for $Cu_{0.9}K_{0.1}Fe_2O_4$, while the $CuFe_2O_4$ indicated a value of 21 emu g^{-1}. On the other hand a lower than 10 emu/g was observed for the oxides obtained from oxalate precursors, suggesting that a proper cation distribution has taken place in the spinel oxides prepared from the hydrazine method. However, the oxalate precursors of these oxides when decomposed at ~320°C in a controlled atmosphere of a known partial pressure of water vapor (N_2/H_2O/Air) showed higher values of 28 and 38 emu g^{-1}, respectively, for $Cu_{0.9}K_{0.1}Fe_2O_4$ and $CuFe_2O_4$. Controlled atmosphere of moisture is crucial in stabilizing γ-type phase as observed in $FeC_2O_4{\cdot}2H_2O$ [1] which easily decomposed to γ-Fe_2O_3 in a known partial pressure of moisture, while in the absence of such atmosphere the product was mainly α-Fe_2O_3.

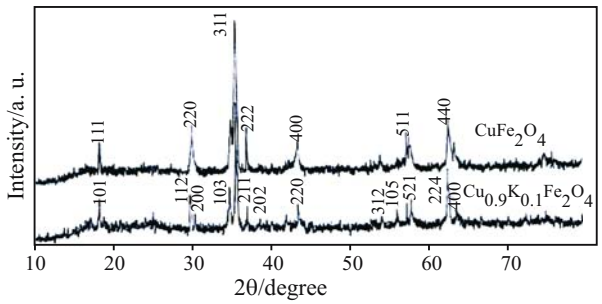

Fig. 3 X-ray diffraction patterns of copper ferrite and K doped copper ferrite obtained from oxalate hydrazinate precursors

Consideration of this aspect of stabilization of the γ-type of phase was our concern [1–8] and the hydrazine modified precursors found easily stabilize the phase, as the desired partial pressure of moisture was provided by the reaction products. However, in hydrazine complexes the hydrazine liberated at lower temperature reacts with the atmospheric oxygen liberating lot of energy [28],

$$N_2H_4+O_2 \rightarrow N_2+2H_2O;\ \Delta H = -625\ \text{kJ mol}^{-1} \quad (1)$$

The energy thus liberated is sufficient for oxidative decomposition of the dehydrazinated complex and the reaction products, N_2+H_2O, provide the necessary environment of desired partial pressure to stabilize the γ-type phase formation. The, in situ supply of heat by coupled exothermic reaction of hydrazine with oxygen, along with the formation of protective layer of nitrogen and moisture surrounding each particle as a result of reaction product is the key for stabilizing the meta stable γ-type phase. Thus, externally controlled partial pressure of moisture during the decomposition of the oxalate precursors of $Cu_{0.9}K_{0.1}Fe_2O_4$ and $CuFe_2O_4$ and in situ supply of the desired partial pressure in hydrazine complexes lead to γ-type phase. The lower saturation magnetization values observed in the ferrite prepared from hydrazine complex required some explanation. The explosive nature of the reaction locally overheats the particle as the protective layer of moisture may not be sufficient for individual particle now acting as micro reactors and the γ-type phase of few particle may transform into α-type.

$(MnZn)Fe_2O_4$ system

The DSC-TG traces of the oxalate show, Fig.4, an endothermic peak ~218°C that followed by an intense exothermic peak ~275°C, while the hydrazinate complex indicates a broad exotherm in the entire range of temperature, 140–315°C, with a peak positioned at ~185°C. The dehydration followed by decarboxylation is the thermal path for the oxalate, while the dehydrazination and decarboxylation are simultaneous processes in the case of hydrazinate complex. Hydrazine complex yields the spinel phase at

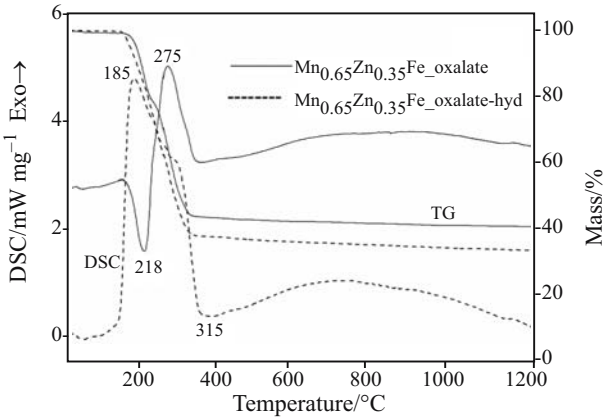

Fig. 4 TG/DSC plots of Mn–Zn Fe-oxalate/oxalate hydrazinate

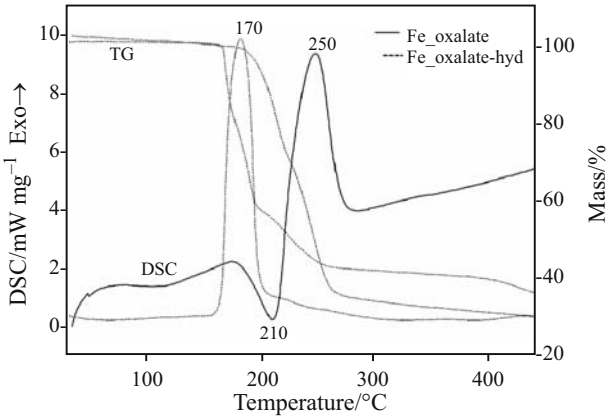

Fig. 5 TG/DSC plots of Fe-oxalate/oxalate hydrazinate

much lower temperature of about 315°C than that of the oxalate complex which requires more than 350°C, the decomposition products of the oxalate at ~350°C however, show admixture of spinel phase and unreacted Fe_2O_3. Although the spinel formation occurs at lower temperatures in the case of hydrazine method, the saturation magnetization value of 41 emu/g that observed is much lower than the value of 60–80 emu g^{-1} expected for the ferrite, while the ferrite from oxalate showed mixed phases and saturation magnetization of <10 emu g^{-1}. The lower value may be due to the lack of proper cation distribution and also possibly some Mn^{2+} ions may have oxidized to Mn^{3+} in explosive decomposition of hydrazine precursor. However, a value of 66 emu/g , which is close to 60 emu/g for nanosize $Mn_{0.65}Zn_{0.35}Fe_2O_4$ [29], could be realized for the ferrite synthesized from the oxalate precursor under controlled atmosphere of moisture at ~350°C and then heated at 900°C at a very low partial pressure of oxygen ($pO_2 \approx 10^{-9}$–10^{-15}) [30].

γ-Fe_2O_3 system

The DSC-TG traces of $FeC_2O_4 \cdot 2H_2O$ (Fe_oxalate), Fig. 5, show an endothermic peak at ~210°C followed immediately by an intense exothermic peak at ~250°C, while $FeC_2O_4 \cdot 2N_2H_4$ (Fe_oxalate_hyd), exothermically decomposes in the entire range of 150–200°C. The decomposition product of the oxalate is hexagonal corundum nonmagnetic α-Fe_2O_3 [1–2] and that of hydrazine complex is the mixture of magnetic cubic spinel, γ-Fe_2O_3, and α-Fe_2O_3. On the other hand, the hydrazine complex, spread on Petri dish, when ignited with a burning splinter it catches fire and a glow forms that then spreads through out the bulk in an ordinary atmosphere, thereby, decomposing autocatalytically mostly into γ-Fe_2O_3 [2].

TiO_2 system

Titanium hydroxide

The TG-DSC traces of titanium hydroxide, $TiO(OH)_2 \cdot 2.5H_2O$,(TiOH) and its hydrazinates $TiO(OH)_2 \cdot 1N_2H_4$ (UH), [TiOH_hyd(UH)] and $TiO(OH)_2 \cdot 4N_2H_4$ (SH), [TiOH_hyd(SH)] are shown in Fig. 6a. All show an endothermic peak ~115°C. The endothermic process in $TiO(OH)_2 \cdot 2.5H_2O$ is then followed by an exothermic peak ~408°C which suggest that the dehydration is followed by dehydr-

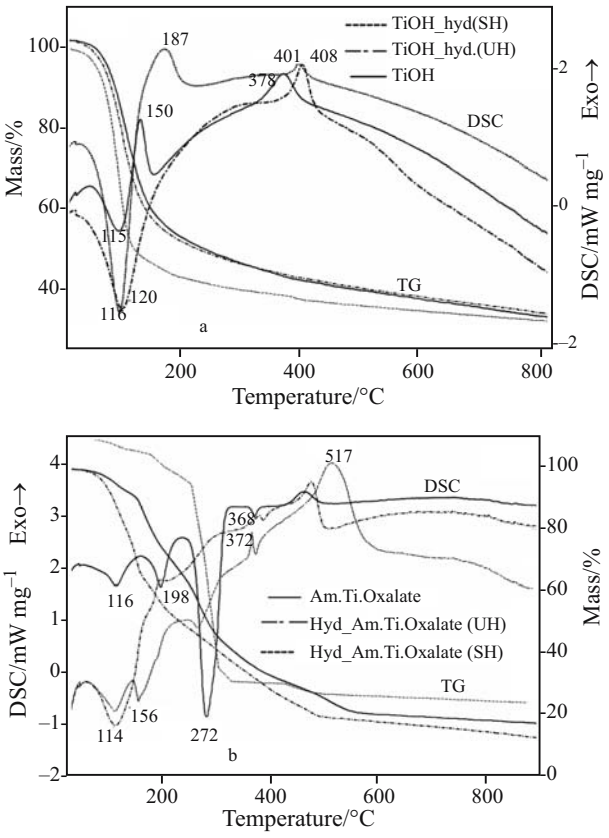

Fig. 6 TG/DSC plots of a – titanium hydroxide/hydrazinate, b – titanium oxalate/oxalate-hydrazinate

oxylation. Though the dehydroxylation occurs at ~400°C, the hydroxyl groups still persist in the case of titanium hydroxide prepared by the precipitation of titanium chloride with ammonia, while the hydroxide prepared by the hydrolysis of titanium isopropoxide completes its dehydroxylation below 500°C, Fig. 1. The hydrazinate complex $TiO(OH)_2 \cdot 1N_2H_4$, however, shows an endothermic peak ~115°C followed immediately by an exothermic peak ~150°C and then there occurs another exothermic peak ~378°C. Here the first endothermic is found to be due to dehydrazination as the product that obtained by isothermally heating the sample at ~100°C showed no presence of hydrazine in it. The two consecutive exothermic processes are indicative of exothermic dehydroxylation. The endothermic peak at ~115°C that followed by exothermic peaks ~187 and 401°C in $TiO(OH)_2 \cdot 4N_2H_4$ too shows that hydrazine modified hydroxide behaves differently as compared to the hydroxide. The thermal products in all these cases yielded well crystalline anatase, TiO_2, at ~400°C as shown in Fig. 7 by a XRD pattern of anataseTiO_2. Hydrazine method does show lower temperature decomposition and the anatase formed by this method yields yellow color nitrogen doped TiO_2, $TiO_{2-x}N_x$, [9], while the white pigment grade oxygen deficient nonstoichiometric TiO_{2-x} was the thermal product of the titanium hydroxide. Thus, the hydrazine method not only reduces the temperature of decomposition, but also produces yellow color N-doped visible light sensitive $TiO_{2-x}N_x$ photocatalyst.

Titanium oxalate

The TG-DSC traces of $(NH_4)_2[TiO(C_2O_4)_2] \cdot H_2O$, (Am.Ti.Oxalate), $(N_2H_5)_2[TiO(C_2O_4)_2]$. N_2H_4 (UH) [Hyd_Am.Ti.Oxalate(UH)] and $(N_2H_5)_2[TiO(C_2O_4)_2] \cdot 3N_2H_4$ (SH) [Hyd_Am.Ti. Oxalate(SH)] are shown in Fig. 6b. (Am.Ti.Oxalate) decomposes giving endothermic peaks at ~114, 198, 272 and 368°C and then exothermic peak at ~500°C. The hydrazine complex prepared under hydrazine method, [Ti_Oxalate_hyd (UH)], shows an endothermic reaction giving peak at ~114°C and then undergoes continuous exothermic process that peaks at ~505°C, while the one prepared synthetically, [Ti_Oxalate_hyd(SH)], indicates endothermic peaks at ~114, 156 and 270°C and then a small exothermic peak at ~372°C that followed by an intense exothermic peak at ~517°C. The thermal product of all these complexes is anatase TiO_2 and the hydrazine complexes yield yellow color N-doped $TiO_{2-x}N_x$ [9]. The XRD pattern of these shows an anatase type phase as in Fig. 7. The nanosize particles are observed in the thermal product of hydrazine complex, whereas, agglomerated particles are found for the decomposed product of oxalate. The TEM of these are shown in Fig. 8. The explosive nature of the low temperature decomposition of the hydrazine complex may be the reason for producing nanosize particles.

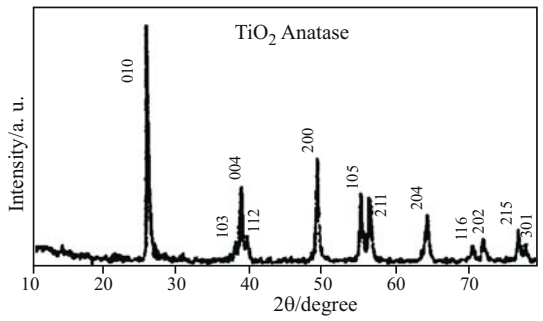

Fig. 7 XRD of anatase TiO_2

Perovskite system

$BaTiO_3$

The DSC-TG curves of $Ba[TiO(C_2O_4)_2] \cdot 6H_2O$, (BaTi_oxalate) show, Fig. 9, an endothermic peak corresponding to dehydration at ~100°C followed by an exothermic peak at ~487°C. In case of hydrazinate complex, $Ba[TiO(C_2O_4)_2] \cdot 7N_2H_4$, (BaTi_oxalate_hyd) an endothermic peak at ~98°C is followed by a sharp exothermic peak at ~203°C and a broad exotherm in the temperature range 210–400°C. There occurs a small exothermic hump ~450°C. The isother-

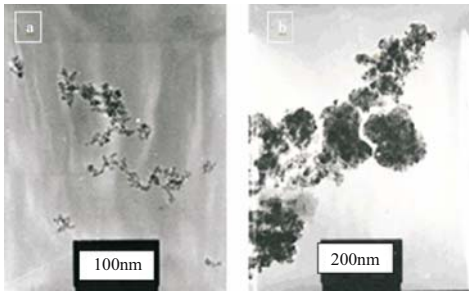

Fig. 8 TEM of TiO_2 obtained from a – oxalate hydrazinate, b – oxalate

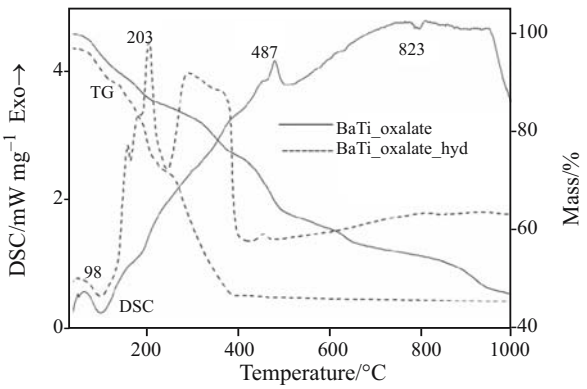

Fig. 9 TG/DSC plots of BaTi oxalate/oxalate-hydrazinate

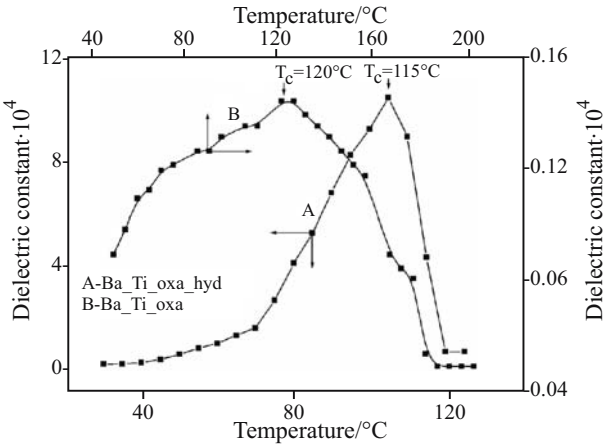

Fig. 10 Dielectric constant of A – Ba Ti oxalate hydrazinate, B – Ba Ti oxalate

mal studies reveal the $BaTiO_3$ formation at ~450°C in hydrazine complex, while the oxalate complex requires a higher temperature of about 500°C to give the perovskites. The variation of dielectric constant as a function of temperature plots, Fig. 10, of the ferroelectric $BaTiO_3$ shows an increase in the value with the increase in the temperature up to 115°C and then decreases sharply to zero in the case of the oxide synthesized by hydrazine method. The sample prepared by oxalate route, however, shows a peak ~120°C, but the increase, as well as the decrease is broad. The Curie temperature thus obtained is as expected for $BaTiO_3$ and since a sharp increase and decrease in the dielectric constant observed in the oxide prepared by hydrazine route suggests superiority of hydrazine method.

$LaCoO_3$, $LaAlO_3$ and $GdCoO_3$

The oxalate and oxalate hydrazinate precursors of $LaAlO_3$, $La_{0.65}Sr_{0.35}AlO_3$, $La_{0.8}Sr_{0.2}CoO_3$ and $La_{0.7}Sr_{0.3}MnO_3$ and $GdCoO_3$ have been synthesized and their thermal decomposition paths have been analyzed [30]. The chemical formulas of few of these precursors are shown in Table 1. The general trend is that the hydrazine complexes show the thermal path different from the oxalate ones, as discussed above. We are not discussing all those here in this paper. However some of the superior behavior of few oxides prepared by the hydrazine method is being described here.

Single phase cubic $LaAlO_3$, Fig. 11, could be obtained at 1000°C from $LaAl(C_2O_4)_3{\cdot}N_2H_4{\cdot}3H_2O$, while >1400°C is required to achieve the phase for oxalate complex, as well as, for the stoichiometric mixture of La_2O_3 and Al_2O_3. In the figure the highlighted by arrows in the XRD pattern for the sample heated below 900°C are due to La_2O_3 impurity. On the other hand, the Sr doped complex, $La_{0.65}Sr_{0.35}Al(C_2O_4)_3{\cdot}2N_2H_4$ heated at 1000°C shows

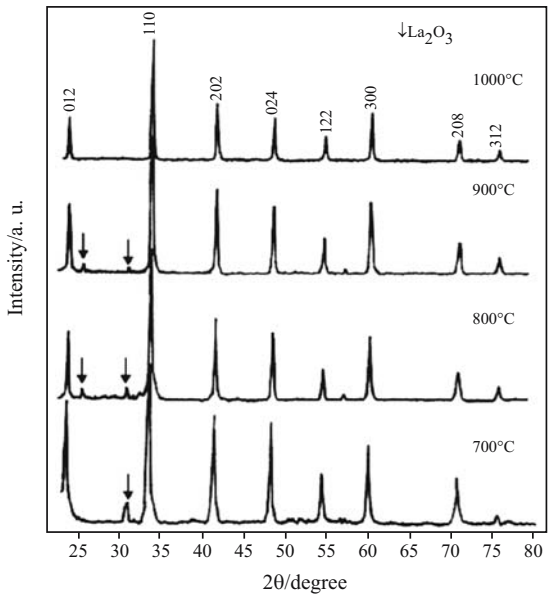

Fig. 11 XRD pattern of $LaAlO_3$

mixed phases, (not shown here) of the perovskite and La_2O_3. However, the single phase cubic $La_{0.65}Sr_{0.35}AlO_3$ could be obtained at ~1500°C. $LaAlO_3$ is a material used as a substrate for depositing thin films of compatible oxides of superconducting nature and ferroelectric materials and hence the formation of well dense $LaAlO_3$ at ~1000°C from the hydrazine method is quite promising one, as otherwise the ceramic technique using La_2O_3 and Al_2O_3 needs very high temperature, >1400°C [31]. The variation of dielectric constant measured at different temperatures and frequencies, Fig. 12 reveal that dielectric constant of $LaAlO_3$ has no measurable change in frequency up to 325°C in all frequencies studied from 1 KHz to 1 MHz and the value of 25 observed is close to the expected values of 20–25 [32, 33]. $La_{0.65}Sr_{0.35}AlO_3$, on the other hand, shows the temperature independent dielectric constant of 50 up to 175°C at 1 KHz and 25 till 350°C at 1 MHz, and there appears decrease in dielectric constant with the increase in frequency 1 KHz to 1 MHz. Slightly distorted perovskites $La_{0.8}Sr_{0.2}CoO_{3-\delta}$ with rhombohedral structure could be achieved from oxalate hydrazinate, $La_{0.8}Sr_{0.2}Co(C_2O_4)_3{\cdot}2N_2H_4{\cdot}3H_2O$ ~1000°C, Fig. 13, while the oxalate complex gave no single phase perovskites at this temperature. The electronic conductivity (S cm^{-1}) measured by Van der Pauw method indicated that there occurs insulator-metal (IM) phase change, Fig. 14, around 500 K [34–36] in the $La_{0.8}Sr_{0.2}CoO_{3-\delta}$. However, an oxygen ion conductivity of $1.995{\cdot}10^{-2}$ (ohm cm)$^{-1}$ observed for $La_{0.8}Sr_{0.2}CoO_3$ at ~700°C is comparatively much higher as compared to that observed by Wiemhoefer *et al.* [37] of $4.6{\cdot}10^{-5}$ (ohm cm)$^{-1}$.

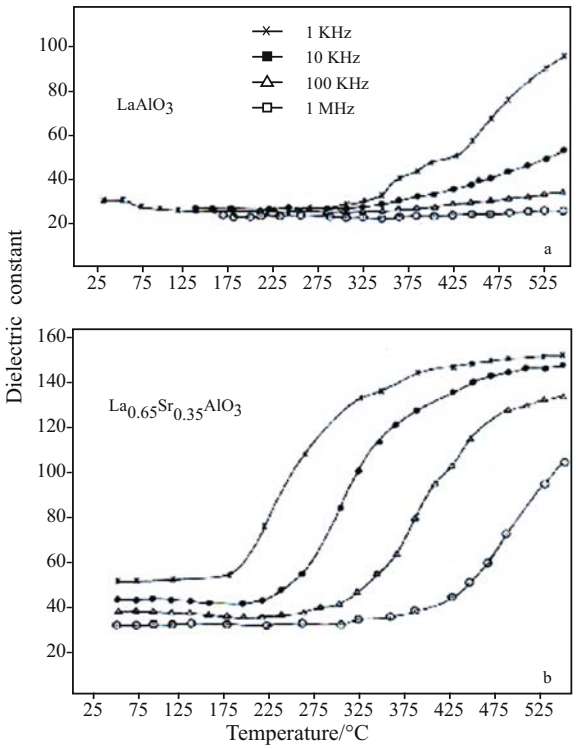

Fig. 12 Dielectric constant *vs.* temperature of a – $LaAlO_3$ and b – $La_{0.65}Sr_{0.35}AlO_3$

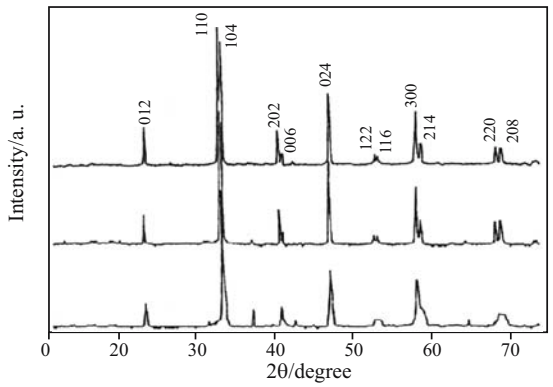

Fig. 13 XRD of $La_{0.8}Sr_{0.2}CoO_3$

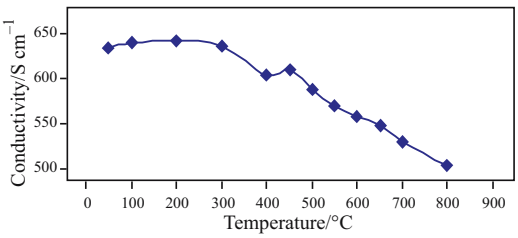

Fig. 14 Electronic conductivity of $La_{0.8}Sr_{0.2}CoO_3$

A gradual IM transition from 500–700 K have been studied [36] by systematic replacement of the R-site in $RCoO_3$, where *R*=La/Pr/Nd/Sm/Eu/Gd. These studies were done on the single crystals and since we observed easy formation of the $LaCoO_3$ and Sr doped $LaCoO_3$ by hydrazine method, we wanted to extend our preparative method in the above series of the perovskites. And here we are describing the single phase $GdCoO_3$ and Ca/Sr/Ba doped $GdCoO_3$ by hydrazine method.

$GdCoO_3$ system

Chemical formulas of citrate and their hydrazinates have been confirmed by elemental, IR and isothermal total mass loss studies and they are as follows: $GdCo(C_6H_5O_7)_2{\cdot}2H_2O$, $GdCo(C_6H_5O_7)_2{\cdot}4N_2H_4$, $Gd_{0.8}Ca_{0.2}Co(C_6H_5O_7)_2{\cdot}10H_2O$, $Gd_{0.8}Ca_{0.2}Co(C_6H_5O_7)_2{\cdot}4N_2H_4$, $Gd_{0.8}Ba_{0.2}Co(C_6H_5O_7)_2{\cdot}10H_2O$, $Gd_{0.8}Ba_{0.2}Co(C_6H_5O_7)_2{\cdot}4N_2H_4$. The TG/DSC traces of all these indicate a modification in thermal path with hydrazination, Figs 15a–d. The thermal products of hydrazinate complexes of all these complexes give single phase perovskites at the end of the complete decomposition temperatures, while in the case of citrates further heating is needed to achieve the perovskite after the complete decomposition.

Significance of the hydrazine method of synthesis

The path of decomposition is found to be modified by hydrazinating the hydroxide, oxalate and citrate precursors of the oxide systems studied in the present investigations. In general the hydrazine complexes decompose at lower temperatures than that without the modification. The dehydration is followed by dehydroxylation in the case of hydroxides and the dehydration is followed by decarboxylation in carboxylates, while it is the dehydrazination that is followed by dehydration/dehydroxylation and dehydration/ decarboxylation in the hydrazinated hydroxide and carboxylates, respectively. The dehydrazination that takes place at lower temperatures makes all the differences in the thermal paths of the hydrazinated complexes. It is the hydrazine that is released reacts with the atmospheric oxygen and liberates enormous energy [28], Eq. (1). And this energy is sufficient to oxidative decomposition of the complex devoid of hydrazine, while the complexes without such hydrazine modification have no such an additional energy to decompose and hence they may be decomposing at much lower temperatures. However, it is the reaction products of hydrazine, N_2+H_2O, that provide the required partial pressure of moisture during the decomposition of the $FeC_2O_4{\cdot}2N_2H_4$ [3] to stabilize the γ-Fe_2O_3, as its importance is observed in the thermal decomposition of $FeC_2O_4{\cdot}2H_2O$ [1]. This is due to the fact that $FeC_2O_4{\cdot}2H_2O$ decomposes in air giving mainly non-magnetic α-Fe_2O_3,

$$FeC_2O_4{\cdot}2H_2O \xrightarrow{-H_2O} FeC_2O_4 \xrightarrow{CO/CO_2} (FeO \rightarrow Fe_2O_4 \rightarrow \gamma\text{-}Fe_2O_3) \xrightarrow{\Delta} \alpha\text{-}Fe_2O_3 \quad (2)$$

On the other hand, the decomposition of the $FeC_2O_4{\cdot}2H_2O$ in an inert atmosphere gives Fe_3O_4, while in a controlled atmosphere of a known partial pressure of moisture the stabilization of γ-Fe_2O_3 takes place

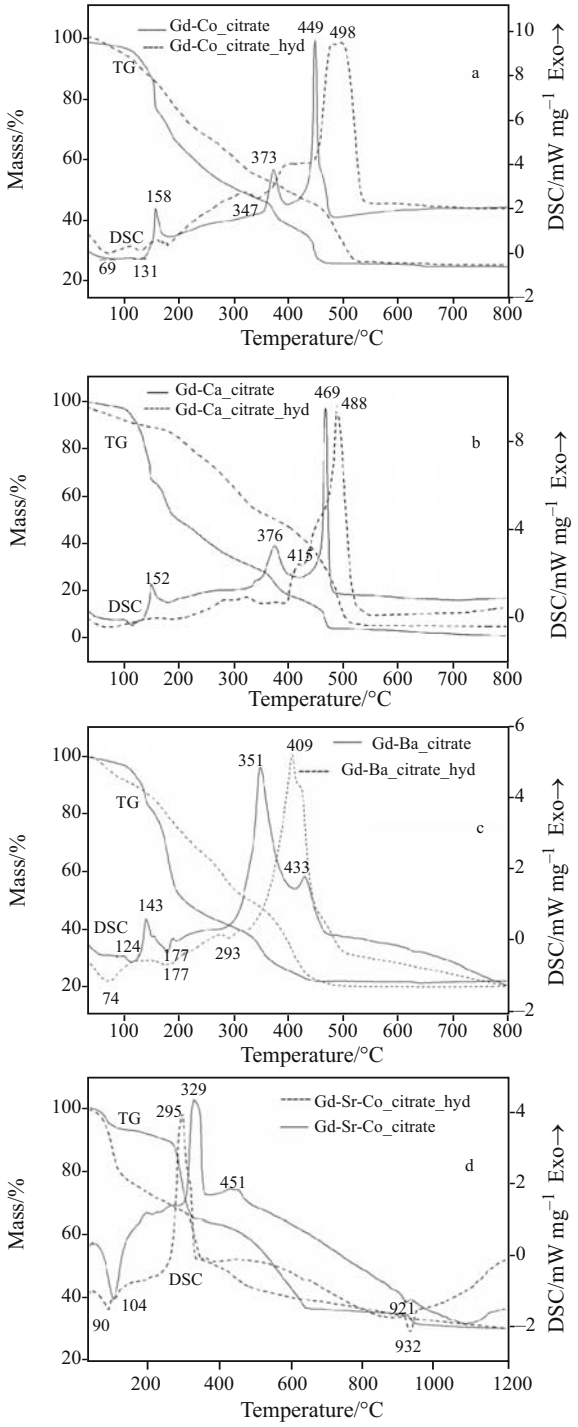

Fig. 15 a, b, c, d TG/DSC plots of Gd (Ca,Ba,Sr)Co-citrate/citrate hydrazinate

$$Fe_3O_4 \xleftarrow{N_2} FeC_2O_4{\cdot}2H_2O \xrightarrow{N_2/H_2O/Air} \gamma\text{-}Fe_2O_3 \quad (3)$$

And, therefore, $FeC_2O_4{\cdot}2N_2H_4$ during its decomposition easily gets the desired partial pressure of moisture from the reaction products of hydrazine, as well as the thermal products of the oxalate, CO/CO_2, to stabilize the γ-Fe_2O_3. The energy released by the hydrazine reaction with atmospheric oxygen (Eq. (1)) may be the reason for the easier low temperature decomposition of the hydrazine complexes, but the formation of yellow color nitrogen doped $TiO_{2-x}N_x$ from the hydrazine complexes of hydroxide and oxalate [9] has to be invoked separately. No doubt the hydrazine helps in lowering the decomposition temperature of these complexes, but here the nitrogen that is being formed in hydrazine break up may be getting trapped in the lattice of the titanium oxide. An observation of the N1s peak ~400 eV (Binding energy) in XPS studies of $TiO_{2-x}N_x$, Fig. 16 and nitrogen content of 0.95% estimated using the oxygen-nitrogen analyzer [16] further supports [9] the introduction of the nitrogen in the TiO_2 by hydrazine method.

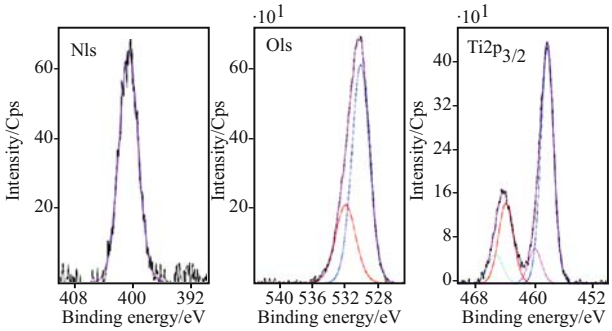

Fig. 16 XPS of N doped TiO_2

Conclusions

- Hydrazine modified hydroxide and carboxylate precursors of the oxide systems: γ-Fe_2O_3, $(MnZn)Fe_2O_4$, $CuFe_2O_4$, $BaTiO_3$, $La(Sr)MnO_3$, $La(Sr)AlO_3$, $La/Gd(Ca/Ba/Sr)CoO_3$, and anatase TiO_2 decompose at low temperatures giving single phase oxide as compared to the ones without such modification.
- Hydrazine released at low temperature during the thermal decomposition reacts with the oxygen in the atmosphere releasing enormous energy,

  $N_2H_4+O_2 \rightarrow N_2+H_2O$; $\Delta H = -625$ kJ mol^{-1}

  that is sufficient for the oxidative decomposition of the hydrazine devoid hydroxide and carboxylate complexes, as compared to the simple hydroxide and carboxylates.
- The reaction products of hydrazine reaction with oxygen not only provide the desired partial pres-

sure of moisture that needed for stabilizing the γ-Fe_2O_3, but also help to incorporate the nitrogen in the lattice of TiO_2 to yield yellow color N-doped $TiO_{2-x}N_x$ photocatalyst.

Acknowledgements

KSR thanks German Academic Exchange Service (DAAD) for awarding NETZSCH DSC-TG STA 409PC equipment under its Global Equipment Grants program (DAAD-Sachmittelprogramm/Gerätespendenprogramm; ref.432a@daad.de) and Department of Science and Technology (DST), New Delhi, for supporting further to add NETZSCH DTA carrier to the equipment under major project grant (Dr. Srinivasan/KSR). Thanks are also due to University Grants Commission (UGC), New Delhi, for financial assistance to RM. KSR also acknowledges the financial support of UGC and DST to the Department of Chemistry, Goa University, under the UGC-Special Assistance Program and DST-FIST program.

References

1 K. S. Rane, A. K. Nikumbh and A. J. Mukhedkar, J. Mater. Sci., 16 (1981) 2387.
2 V. Borker, K. S. Rane andV. N. Kamat Dalal, J. Mater. Sci. Mater. Electr., 4 (1993) 241.
3 K. S. Rane and V. M. S. Verenkar, Bull. Mater. Sci., 24 (2001) 39.
4 K. S. Rane, V. M. S. Verenkar and P. Y. Sawant, Bull. Mater. Sci., 24 (2001) 331.
5 V. Moye, K. S. Rane and V. N. Kamat Dalal, J. Mater. Sci. Mater. Electr., 1 (1990) 212.
6 K. S. Rane, V. M. S. Verenkar and P. Y. Sawant, J. Mater. Sci. Mater. Electr., 10 (1999) 133.
7 K. S. Rane, V. M. S. Verenkar and P. Y. Sawant, Mater. Sci., 24 (2001) 323.
8 K. S. Rane, V. M. S. Verenkar, R. M. Pednekar and P. Y. Sawant, J. Mater. Sci. Mater. Electr., 10 (1999) 121.
9 K. S. Rane, R. Mhalsiker, S. Yin, T. Sato, K. Cho, E. Dunbar and P. Biswas, J. Solid State Chem., 179 (2006) 3033.
10 R. Mhalsikar, R. Pednekar and K. S. Rane, Electrical Characteristics of TiO_2 synthesized from different precursors, Inorganic Materials: Recent Advances. Eds: D. Bahadur, S. Vitta, Om Prakash, Narosa Publishing House, New Delhi, India (Paper presented at the International Symposium in Inorganic Chemistry, IIT-Bombay, Mumbai, India, Dec. 11–13 2002) pp. 469–471.
11 H. Zhu, D. Yang, G. Yu, H. Zhang and K. Yao, Nanotechnology, 17 (2006) 2386.
12 Y. Jiang, Y. Wu, B. Xie, S. Zhang and Y. Qian, Nanotechnology, 15 (2004) 283.
13 J. Y. Kim, M. A. Sriram, P. H. McMichael, P. N. Kumta, B. L. Phillips and S.H. Risbud, J. Phys. Chem. B, 101 (1997) 4689.
14 J. H. Zhan, Y. Xie, X. G. Yang, W. X. Zhang and Y. T. Qian, J. Solid State Chem., 146 (1999) 36.
15 I. A. Vogel, A Text Book of Quantitative Inorganic Analysis, Longman, UK 1978.
16 S. Yin, H. Yamaki, M. Komatsu, Q. Zhang, J. Wang, Q. Tang, F. Saito and T. Sato, J. Mater. Chem., 13 (2003) 2996.
17 S. D. Likhite, C. Radhakrishnamurthy and P. W. Sahasrabudhe, Rev. Sci. Instrum., 36 (1965) 1558.
18 L. G. Van der Pauw, Philips Research Reports, 13 (1958) 1; A. A. Ramadan, R. D. Gould nad A. Ashour, Thin Solid Films, 239 (1994) 272.
19 A. Braibanti, F. Dallavalle, M. A. Pellinghelli and E. Leporati, Inorg. Chem., 7 (1968) 1430.
20 A. Yasodhai and S. Govindarajan, J. Therm. Anal. Cal., 67 (2002) 679.
21 L. Sacconi and A. Sabatini, J. Inorg. Nucl. Chem., 25 (1963) 1389.
22 A. Earnshaw, L. F. Larkworthy and K.S. Patel, Z. Anorg. Allg. Chem., 334 (1964) 163.
23 W. G. Patterson and M. Onyszchuk, Can. J. Chem., 41 (1963) 1872.
24 J. N. Kim, M. A. Sriram, P. H. McMichael, P. N. Kumta, B. L. Phillips and S. H. Risbud, J. Phys. Chem. B., 101 (1997) 4689.
25 M. S. Bains and D. C. Bradley, Can. J. Chem., 40 (1962) 1350.
26 Y. Gao, Y. Masuda, Z. Peng, T. Yonezawa and K. Koumoto, J. Mater. Chem., 13 (2003) 608.
27 T. Lopez, J. A. Moreno, R. Gomez, X. Bokhimi, J. A. Wang, H. Yee-Madeira, G. Pecchi and P. Reyes, J. Mater. Chem., 12 (2002) 714.
28 E. W. Schmidt, Hydrazine and its Derivatives-Preparation, Properties and Applications, Wiley Interscience New York 1984.
29 C. Rath, N. C. Mishra, S. Anand, R. P. Das, K. K. Sahu, U. Chandan and H. C. Verma, Appearance of superparamagnetism on heating nanosize $Mn_{0.65}Zn_{0.35}Fe_2O_4$', (adsabs.harvard.edu/abs/ 2000ApPhL.. 76..475R), Applied Phys. Letters, 76 (2000) 475.
30 R. M. Pednekar, 'Synthesis and characterization of metal and mixed metal oxides of spinel and perovskite structure', Ph.D. Thesis Goa Univeristy, Goa, India 2006.
31 G. Y. Sung, K. Y. Kong and S.-C. Park, J. Am. Ceram. Soc., 74 (1991) 437.
32 B.-E. Park and H. Ishiwara, Appl. Phys. Lett., 82 (2003) 1197.
33 P. Delugas, V. Fiorentini and A. Filippeti, Phys. Rev. B., 71 (2005) 134302.
34 S. Yamaguchi, Y. Okimoto and Y. Tokura, Phys. Rev. B., 55 (1997) R8666.
35 S. Yamaguchi, Y. Okimoto, H. Taniguchi and Y. Tokura, Phys. Rev. B., 53 (1996) R2926.
36 S. Yamaguchi, Y. Okimoto and Y. Tokura, Phys. Rev. B., 54 (1996) R11 022.
37 W. Zipprich, S. Waschilewski, F. Rocholl and H. D. Wiemhoefer, Solid State Ionics, 101–103 (1997) 1015.

DOI: 10.1007/s10973-007-8515-8